



HAL
open science

Structural Control on Downtip Locking Extent of the Himalayan Megathrust

Eric Lindsey, Rafael Almeida, Rishav Mallick, Judith Hubbard, Kyle Bradley, Louisa Tsang, Yixiang Liu, Roland Bürgmann, Emma Hill

► **To cite this version:**

Eric Lindsey, Rafael Almeida, Rishav Mallick, Judith Hubbard, Kyle Bradley, et al.. Structural Control on Downtip Locking Extent of the Himalayan Megathrust. *Journal of Geophysical Research : Solid Earth*, 2018, 123 (6), pp.5265-5278. 10.1029/2018jb015868 . hal-02353888

HAL Id: hal-02353888

<https://hal.science/hal-02353888>

Submitted on 1 Nov 2021

HAL is a multi-disciplinary open access archive for the deposit and dissemination of scientific research documents, whether they are published or not. The documents may come from teaching and research institutions in France or abroad, or from public or private research centers.

L'archive ouverte pluridisciplinaire **HAL**, est destinée au dépôt et à la diffusion de documents scientifiques de niveau recherche, publiés ou non, émanant des établissements d'enseignement et de recherche français ou étrangers, des laboratoires publics ou privés.



Distributed under a Creative Commons Attribution - NonCommercial - ShareAlike 4.0 International License

RESEARCH ARTICLE

10.1029/2018JB015868

Key Points:

- The limit of fault coupling on the Main Himalayan Thrust agrees with geologic models of the midcrustal ramp in central and eastern Nepal
- In western Nepal, the fault coupling transition falls between two proposed ramp locations, and we suggest that both may be active
- The moment accumulation rate in our model is 30% smaller than previous results, partially resolving an apparent seismic moment deficit

Supporting Information:

- Supporting Information S1
- Data Set S1

Correspondence to:

E. O. Lindsey,
 elindsey@ntu.edu.sg

Citation:

Lindsey, E. O., Almeida, R., Mallick, R., Hubbard, J., Bradley, K., Tsang, L. L. H., et al. (2018). Structural control on downdip locking extent of the Himalayan megathrust. *Journal of Geophysical Research: Solid Earth*, 123, 5265–5278. <https://doi.org/10.1029/2018JB015868>

Received 30 MAR 2018

Accepted 28 MAY 2018

Accepted article online 4 JUN 2018

Published online 19 JUN 2018

©2018. The Authors.

This is an open access article under the terms of the Creative Commons Attribution-NonCommercial-NoDerivs License, which permits use and distribution in any medium, provided the original work is properly cited, the use is non-commercial and no modifications or adaptations are made.

Structural Control on Downdip Locking Extent of the Himalayan Megathrust

Eric O. Lindsey¹ , Rafael Almeida¹ , Rishav Mallick^{1,2} , Judith Hubbard^{1,2} , Kyle Bradley¹ , Louisa L. H. Tsang^{1,2,3} , Yixiang Liu² , Roland Burgmann⁴ , and Emma M. Hill^{1,2} 

¹Nanyang Technological University, Earth Observatory of Singapore, Singapore, Singapore, ²Nanyang Technological University, Asian School of the Environment, Singapore, Singapore, ³Now at Géosciences Azur, CNRS, Valbonne, France, ⁴University of California, Department of Earth and Planetary Science, Berkeley, CA, USA

Abstract Geologic reconstructions of the Main Himalayan Thrust in Nepal show a laterally extensive midcrustal ramp, hypothesized to form the downdip boundary of interseismic locking. Using a recent compilation of interseismic GPS velocities and a simplified model of fault coupling, we estimate the width of coupling across Nepal using a series of two-dimensional transects. We find that the downdip width of fault coupling increases smoothly from 70 to 90 km in eastern Nepal to 100–110 km in central Nepal, then narrows again in western Nepal. The inferred coupling transition is closely aligned with geologic reconstructions of the base of the midcrustal ramp in central and eastern Nepal, but in western Nepal, the data suggest that the location is intermediate between two proposed ramp locations. The result for western Nepal implies either an anomalous coupling transition that occurs along a shallowly dipping portion of the fault or that both ramps may be partially coupled and that a proposed crustal-scale duplexing process may be active during the interseismic period. We also find that the models require a convergence rate of 15.5 ± 2 mm/year throughout Nepal, reducing the geodetic moment accumulation rate by up to 30% compared with earlier models, partially resolving an inferred discrepancy between geodetic and paleoseismic estimates of moment release across the Himalaya.

1. Introduction

The latest rupture of the Main Himalayan Thrust (MHT), the 2015 M_w 7.8 Gorkha earthquake, was likely limited in size by changes in the fault geometry along strike and dip (Hubbard et al., 2016). The rupture occurred primarily on a subhorizontal décollement bounded on several or all sides by more steeply dipping ramps (Elliott et al., 2016; Galetzka et al., 2015; Hubbard et al., 2016; Lindsey et al., 2015; Qiu et al., 2016; Wang et al., 2017). The presence of a midcrustal ramp, located to the north of the Gorkha rupture, has long been proposed as a key structural component of the MHT throughout the Nepal Himalaya (e.g., Avouac, 2015; Pandey et al., 1995; Robinson et al., 2006; Schelling & Arita, 1991). If the deeper midcrustal ramp controlled the downdip edge of the rupture, its presence likely affects other parts of the earthquake cycle as well. Here we seek to understand how this structural feature may affect the interseismic locking transition across Nepal.

In a thrust environment, the greatest total uplift will typically be found near the top of thrust ramps (Suppe, 1983), and in Nepal, the exposure of the stratigraphically oldest rocks of the Lesser Himalaya (defined as the core of the Gorkha-Pokhara anticlinorium) provides strong, though indirect, evidence for the location of the top of the midcrustal ramp along strike. The width of this ramp can be estimated from balanced cross sections based on mapped geology (Hubbard et al., 2016). The inferred base of this ramp is denoted as a blue line in Figure 1. The distance between this ramp and the surface trace of the MHT, the Main Frontal Thrust (MFT), varies significantly along strike. These variations imply differences in the structure of the MHT and in the associated seismic hazard. However, the existence of a single ramp is not agreed upon everywhere, particularly where the Gorkha-Pokhara anticlinorium bifurcates in western Nepal. There, evidence from topography, geology, and complex patterns of microseismicity suggest that the MHT is either composed of two ramps linking together three décollement levels (DeCelles et al., 1998), or that a thrust duplex has formed, with two active ramps linking together two décollement levels, one above the other (Harvey et al., 2015).

Geodetic data suggest that the shallow MHT is fully coupled across Nepal; that is, there is zero relative motion across the fault interface during the interseismic period. In central Nepal, the downdip width of this coupled zone has been estimated at close to 100 km (e.g., Freymuller et al., 1996; Grandin et al., 2012;

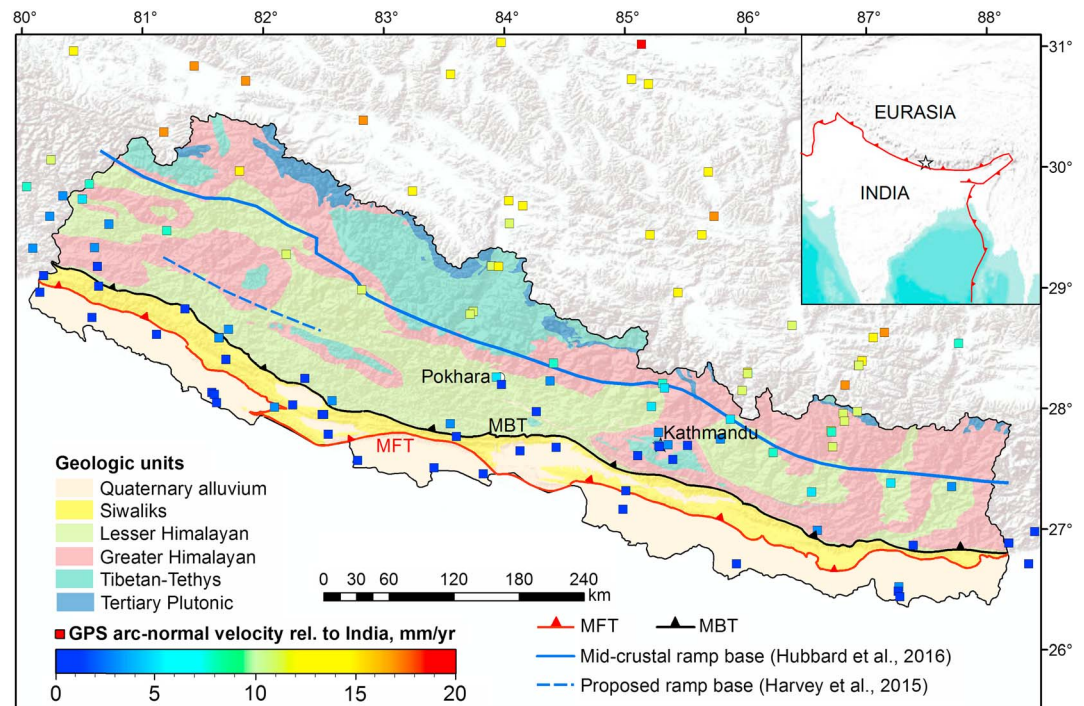


Figure 1. Map showing geologic provinces in Nepal (Department of Mines and Geology of Nepal, 1994), faults active during the Quaternary, and GPS-derived convergence rates relative to India. The solid blue line shows the base of the midcrustal ramp inferred by Hubbard et al. (2016). The dashed blue line in western Nepal indicates the approximate location of the base of the southern ramp proposed by DeCelles et al. (2001) and Harvey et al. (2015). The colored squares show the arc-normal components of GPS velocities in the Indian plate reference frame (Kreemer et al., 2014). The locations of the Main Frontal Thrust (MFT) and Main Boundary Thrust (MBT) are shown in red and black, respectively. Inset shows primary thrust faults between India and Eurasia in red, with Kathmandu shown as a white star.

Jouanne et al., 2004; Larson et al., 1999). In the same area, the downdip edge of the coupled area is correlated with an active band of microseismicity and the geologically inferred ramp location (Ader et al., 2012; Cattin & Avouac, 2000; Pandey et al., 1995; Stevens & Avouac, 2015). However, in eastern and western Nepal, the link between the ramp (or ramps) and the interseismic behavior of the fault has not been as clearly established.

When considering variations along strike, models of interseismic locking in megathrust systems commonly adopt an inversion for slip deficit (or coupling) on small patches of the fault, analogous to a coseismic slip inversion (e.g., Bradley et al., 2017; Bürgmann et al., 2005; Chlieh et al., 2008; Loveless & Meade, 2010; Moreno et al., 2010; Suwa et al., 2006; Wallace et al., 2004). Where the data are sufficiently dense and precise, the inversion can reveal fine details of fault coupling, but this typically requires additional constraints and assumptions, such as spatial smoothing, which make the underlying physical processes difficult to interpret. For example, one recent coupling model in Nepal used the density of microseismicity as a strain-rate marker to modulate the smoothing parameter (Stevens & Avouac, 2015), resulting in a coupling map that correlates well with the microseismicity but which is not independent of it. Inversions for coupling in three dimensions can be useful for hazard analysis, but the use of many free parameters or reliance on additional assumptions makes it difficult to independently assess the underlying physical mechanisms. This is particularly true in areas like western Nepal, where additional geologic complexity suggests that the relationship between structure and coupling is not simple.

One alternative approach is to enforce a smooth coupling distribution by using a model with fewer free parameters, such as a series of finite dislocations (Bettinelli et al., 2006; Jouanne et al., 2004). Here to focus our analysis on variations in the width of coupling along the MHT, we adopt this simplified approach and model a series of two-dimensional (2D) profiles drawn perpendicularly to the fault (Figure S1). We invert each profile separately for the location of a single locked-to-creeping transition at depth using a semi-infinite, 2D dislocation model and compare the results to geologic observations. Like the three-dimensional (3D) coupling

models, this approach is sensitive to the assumed dislocation geometry, which relates nonlinearly to deformation and can cause biases (e.g., Lindsey & Fialko, 2013); we assess the effect of mismodeled geometry in a Bayesian framework to obtain a conservative estimate of the model uncertainty. Our model is independent of the structural data, yet we find that the obtained extent of coupling correlates strongly with both the distribution of microseismicity (Ader et al., 2012) and the geologically inferred base of the midcrustal ramp across central and eastern Nepal (Hubbard et al., 2016). In western Nepal, our inferred coupling transition is located between the two proposed midcrustal ramps (DeCelles et al., 1998; Harvey et al., 2015; Hubbard et al., 2016), which suggests neither ramp is dominant and may indicate partial coupling along the décollement between the two ramps.

2. Methods and Results

To constrain our inversions, we use a recently updated set of GPS velocities spanning the 1990s to 2015, within and surrounding Nepal, including recently updated velocities for Tibet. Site velocities within Nepal and India from a number of published studies were combined into a consistent reference frame by reducing the best-fitting pole of rotation between overlapping sites in each data set by Kreemer et al. (2014); these were combined with a reprocessed, updated velocity field for stations within China by Zheng et al. (2017). The velocities are reported by Zheng et al. (2017) in the Eurasia-fixed reference frame; we used the rotation pole for Eurasia-India motion reported by Kreemer et al. (2014) to convert the velocities to an India-fixed reference frame, then selected all data within 300 km of the MFT. The final 275 velocities within the study region are taken from 16 published studies (Ader et al., 2012; Banerjee et al., 2008; Bettinelli et al., 2006; Gahalaut et al., 2013; He et al., 2013; Ischuk et al., 2013; Jade et al., 2004; Jade et al., 2007; Kreemer et al., 2014; Liang et al., 2013; Mahesh et al., 2012; Mukul et al., 2010; Mullick et al., 2009; Paul et al., 2001; Ponraj et al., 2010; Zheng et al., 2017) and are listed in supporting information Table S1. We did not include leveling (Jackson & Bilham, 1994) or InSAR (Grandin et al., 2012) observations, because these data are available only in two narrow locations along strike and their inclusion would make the resulting data distribution too heterogeneous along strike.

We first construct a smooth approximation to the MFT (supporting information Figure S1) and project the arc-perpendicular velocity components onto 150-km-wide overlapping profiles (supporting information Figure S2). The profiles are narrow enough to render effects due to arc curvature negligible but at the same time wide enough to include sufficient data to recover a robust model fit for each profile. The projection parameters for each profile are listed in supporting information Table S2. We neglected any arc-parallel component of velocity in the modeling since this motion is likely taken up by independent structures within the overriding plate (e.g., Murphy et al., 2014; Silver et al., 2015) and these values are comparatively small (less than 5 mm/year, see Figure S2; also Banerjee et al., 2008). We address possible complications from unmodeled 3D effects related to arc-parallel motion and deformation in Tibet (e.g., McCaffrey & Nabelek, 1998; Zhang et al., 2004) with a separate model in the discussion. The profile locations are shown in map view in Figure S1, and the projected arc-perpendicular and arc-parallel velocities from all profiles are shown in Figure S2.

We then fit a simplified, 2D interseismic dislocation model to each profile, assuming a single, sudden locked-to-creeping transition. The model is an analytic solution relating surface displacements v_i at station positions x_i to slip s on a semi-infinite plane strain dislocation in an elastic half space (Mansinha & Smylie, 1971; Rani & Singh, 1992; Savage, 1980; Segall, 2010):

$$v_i = \frac{S}{\pi} \left(\cos \delta \tan^{-1} \zeta + \frac{\sin \delta - \zeta \cos \delta}{1 + \zeta^2} \right); \quad \zeta = \frac{X_i - d}{D}$$

The free parameters are the long-term slip rate s , the depth to the dislocation D , and the horizontal locking distance from the MFT d . The reference frame for the model is chosen such that the far-field velocity tends to zero in India, by applying a least squares penalty to the absolute value of the modeled velocity at a distance of 500 km south of the fault trace. The dip δ of the dislocation below the coupling transition is held constant in all models. We compared several possible values (0° , 5° , and 10°) and found that variations in dip make only a small change in the result, with a maximum difference of 0.8 mm/year between the models, localized to a ~ 10 -km region around the locking line, but do not impact the velocities in the

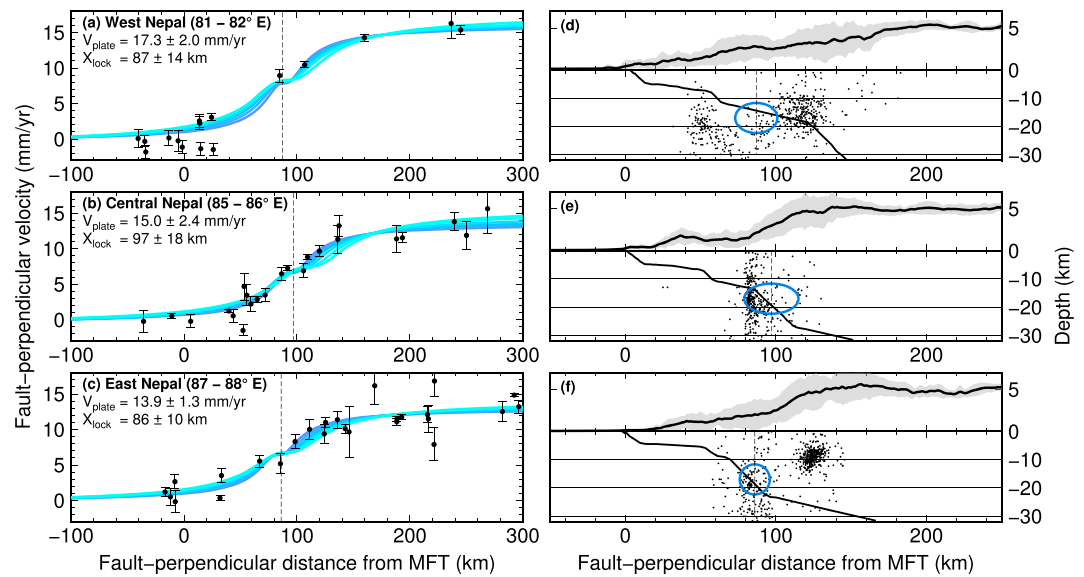


Figure 2. (a–c) Model fit and inferred geometry from three profiles from western (a), central (b) and eastern (c) Nepal. Profile locations are shown in Figure 3. The six blue lines in each profile represent best-fitting models with different assumed depths to the dislocation, sampled every 2 km between 12 (dark blue) and 22 km (light blue). The reported parameter uncertainties represent the combination of all models. (d–f) Vertically exaggerated cross sections showing the inferred position of the dislocation edge with uncertainties (blue ellipses) compared to the modeled Main Himalayan Thrust geometry from Hubbard et al. (2016), along with mean, minimum, and maximum topography along each profile, and observed microseismicity from the relocated Nepal National Seismological Centre catalog (1996–2008; Ader et al., 2012; Rajaure et al., 2013). Results for all profiles are shown in Figure S5. MFT = Main Frontal Thrust.

far field (supporting information Figure S3). Therefore, we set the dip to zero to make the slip rate and plate convergence rate identical. This would be consistent with the dislocation representing a horizontal shear zone or brittle-ductile transition at constant depth. In addition, we created a synthetic model to test the effect of ignoring the small component of fault-parallel motion that would be generated by changes in the locking distance along strike and found no bias in the results even in the case of a step change in locking. However, the scale over which we could resolve such a step is limited by the data profile width (supporting information Figure S4).

Models in which the depth is considered a free parameter tend to prefer extremely shallow depths (in some cases less than 10 km), which we consider unlikely given available observations. We therefore allowed the locked-to-creeping transition to vary in depth from 12 to 22 km below the model surface, in accordance with thermal modeling that proposes this depth range for the brittle-ductile transition in Nepal (Herman et al., 2010). This is consistent with the maximum depth of relocated aftershocks following the 2015 Gorkha event (15 km below sea level; Wang et al., 2017). This range is similar to depths used in previous studies, which used an average fault dip to fix the depth at approximately 17 km below the surface based on a locking distance of 100 km (Ader et al., 2012; Bettinelli et al., 2006; Jouanne et al., 2004; Stevens & Avouac, 2015).

This method allows us to identify the location of greatest geodetic strain rate along each profile, reflecting the fault's downdip transition from locked to creeping. However, the use of a single dislocation should not be understood to imply that we believe the transition from locked to creeping is sudden. Instead, the transition zone must occur over some finite width that is likely controlled by both rheology and temperature on the fault (e.g., Scholz, 1988, 1998; Hyndman, 2013), and its width may depend on the distance over which the temperature increases through the brittle-ductile transition. This in turn depends on several factors, including the dip of the fault (e.g., Bilham et al., 2017). The sensitivity of geodetic data to this transition width is limited, however, due to a nearly perfect trade-off with the depth of locking (Lindsey et al., 2014).

Throughout the discussion below, we use the terms *locked* and *coupled* interchangeably to refer to the updip portion of the fault that is not slipping. We note that by doing so, we implicitly assume that the entire portion of the fault that is not slipping (kinematically coupled) is also frictionally locked and therefore potentially

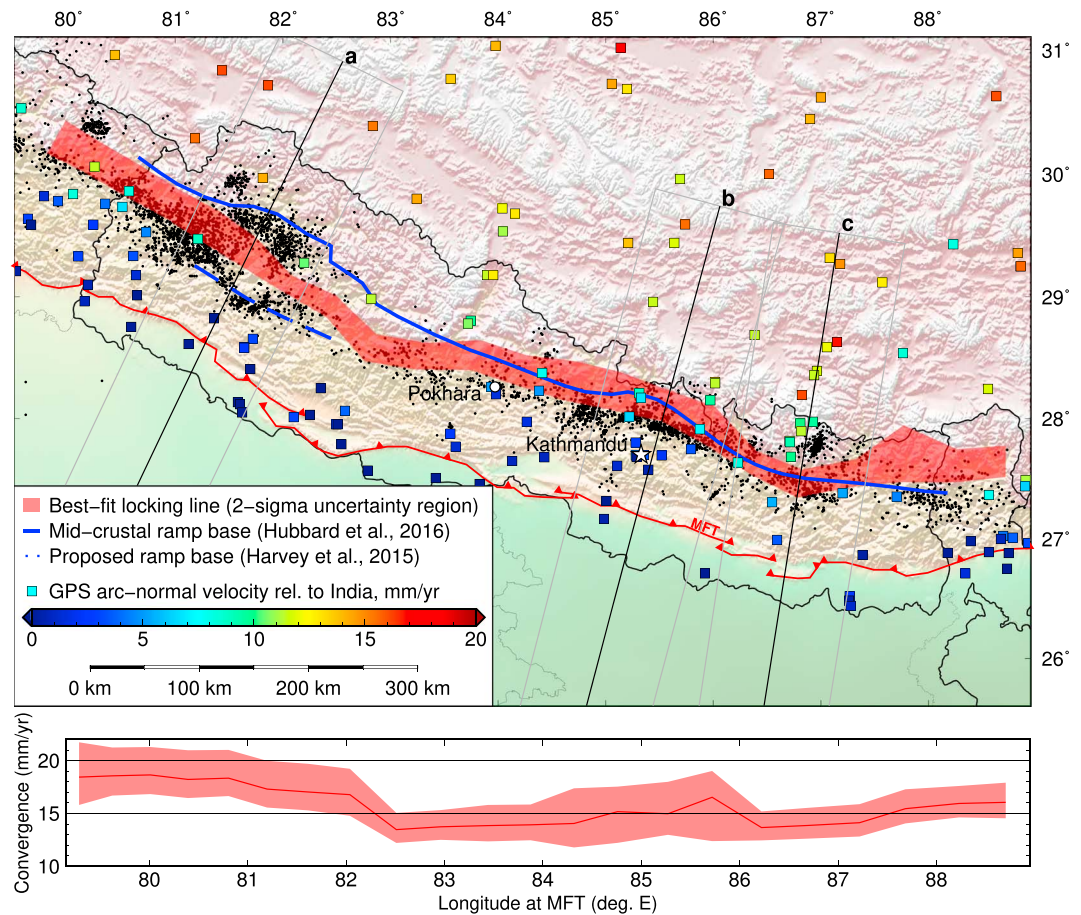


Figure 3. Modeled downdip limit of coupling across Nepal, shown as a red band representing the 95% confidence range. The solid blue line shows the downdip edge of the midcrustal ramp inferred from surface geology (Hubbard et al., 2016); the dashed blue line shows a proposed new ramp structure in western Nepal (Harvey et al., 2015). The colored squares show the arc-normal component of GPS velocities relative to India. Profiles labeled (a), (b), and (c) correspond to the panels in Figure 2; all profile locations are shown in supporting information Figure S1. Black dots denote microseismicity from a relocated Nepal National Seismological Centre catalog (1996–2008; Ader et al., 2012; Rajauri et al., 2013) and from Mahesh et al. (2013). Background colors and shading represent topography. Lower panel shows the best-fitting inferred slip rate (red line) and 95% confidence range (red bar) for each profile along strike. MFT = Main Frontal Thrust.

seismogenic. This is a conservative assumption; some of the presently coupled areas could in fact be frictionally stable (unlocked) and simply located in the stress shadows of nearby locked patches, preventing them from creeping interseismically (Almeida et al., 2018). In this case, they may release their slip deficit as future afterslip rather than as coseismic slip. However, given the absence of shallow afterslip following the 2015 Gorkha earthquake (e.g., Wang & Fialko, 2018) and the lack of evidence for shallow creep, we feel that this conservative assumption is appropriate for the MHT.

The model results for three representative profiles are shown in Figure 2; the complete set is shown in Figure S5, along with the weighted misfit values for each model for each profile. The modeled coupling transition location is compared to topography, microseismicity, and the fault model of Hubbard et al. (2016) in the right-hand panels. Our preferred location for the coupling transition in each profile is shown in map view as the red line in Figure 3, with the red shaded area representing uncertainty. Uncertainties were calculated for all parameters using a Bayesian framework (Lindsey & Fialko, 2013) with uniform prior distributions for all model parameters and by combining all models from the range of possible assumed depths (12–22 km). Figure 3 shows the downdip edge of the midcrustal ramp proposed by Hubbard et al. (2016) for comparison, along with the distribution of microseismicity from the relocated Nepal National Seismological Centre catalog

(Ader et al., 2012; Rajaure et al., 2013). In western Nepal, the southern dashed line shows the location of a proposed southward step of the active ramp of the Lesser Himalayan duplex (Harvey et al., 2015).

The modeled plate convergence rates are shown in the lower panel of Figure 3; the average is 15.5 ± 2 mm/year across Nepal when considering the model uncertainties and the assumed range of possible depths. The inferred rates are generally well constrained by data far from the coupling transition, particularly in Tibet, although the rates do trade off with the modeled depth of the dislocation, and show some variation across Nepal with higher rates in the west. Models with the shallowest assumed depth of 12 km have an average convergence rate of 14.7 ± 2 mm/year, while models with a 22-km depth increase to an average rate of 16.4 ± 2 mm/year. Overall, the rates are lower than commonly cited geologic slip rates of 18–21 mm/year for the MFT in central Nepal (Bollinger et al., 2014; Lavé & Avouac, 2001; Mugnier et al., 2004); we discuss the possible reasons for this difference below.

3. Discussion

3.1. Along-Strike Variations

The location of our modeled locking transition strongly correlates with the geologically inferred ramp in eastern and central Nepal. Here the modeled locking line generally falls near the lower half of the ramp or at its base (Figures 2e and 2f). In the east, both the base of the ramp and the inferred locking line are approximately 80 km from the MFT, making this the narrowest part of the locked zone in Nepal. Geologic observations there suggest a single midcrustal ramp and relatively simple thrust geometry (Hubbard et al., 2016; Schelling & Arita, 1991). This contrasts with nearby central Nepal, where the locked zone is at its widest beneath Kathmandu. It has been suggested that several Gorkha-type moderate earthquakes may be required to sufficiently load the upper part of the fault here, which may explain why the last two large earthquakes occurred only on the deeper, blind part of the fault in 1833 and 2015 (Bilham et al., 2017). By comparison, in eastern Nepal paleoseismic evidence suggests that the past two recorded events (in A.D. 1255 and 1934) ruptured all the way to the surface (Bollinger et al., 2014; Nakata et al., 1998; Sapkota et al., 2013; Wesnousky et al., 2017). Earthquake cycle models incorporating realistic fault geometry have shown that an upper ramp can potentially control the occurrence of partial ruptures (Qiu et al., 2016). An intriguing question, then, is whether the proposed change in structure between central and eastern Nepal also forms a persistent rupture boundary, as has been observed at along-strike structural changes in other subduction zones including Chile and Sumatra (e.g., Melnick et al., 2009; Meltzner et al., 2012; Morgan et al., 2017; Tang et al., 2013).

In western Nepal, the inferred coupling transition passes between the divided northern and southern outcrops of Lesser Himalayan rocks (Figures 1 and 2c). This contrasts with the location of the deep ramp proposed by Hubbard et al. (2016) and Robinson et al. (2006), which follows the northern outcrop of Lesser Himalayan material. However, other authors have suggested that the active ramp falls at the southern outcrop belt (DeCelles et al., 2001). To reconcile these interpretations with an observed broadening of the topographic slope in this area and a double band of microseismicity, Harvey et al. (2015) proposed that both ramps are simultaneously active, reflecting an ongoing process of crustal-scale duplexing. In this scenario, the deep décollement transfers slip to both ramps at a partial rate, leading to elevated strain rates and microseismicity in both areas at the same time (Figure 4b). Our method assumes only a single narrow coupling transition, so we created a synthetic test for the case of a half-coupled décollement between two transition points and found that the model returns a best-fitting location halfway between the two points (supporting information Figure S6), similar to the results obtained for this area. Thus, our results are consistent with an active duplex producing interseismic strain on both ramps, with a décollement slipping interseismically at a reduced rate between them. Crustal-scale duplexing is believed to be an important process during the growth of the Himalaya (e.g., Cannon & Murphy, 2014; Gao et al., 2016), but the combined geologic, microseismic, and geodetic observations suggest that this section of the MHT may be the only area in Nepal where it is presently ongoing. Structural models typically assume that the ramp in the hinterland is abandoned as soon as the new ramp becomes active, but these observations suggest that there may be a prolonged transition period between these two events.

It is also possible that only one ramp is still active or that the two proposed ramps in the west are linking three décollement levels rather than two, in which case this would not represent a duplex but rather a thrust system (e.g., DeCelles et al., 1998; Hubbard et al., 2016). In this case, the geodetic data suggest that the

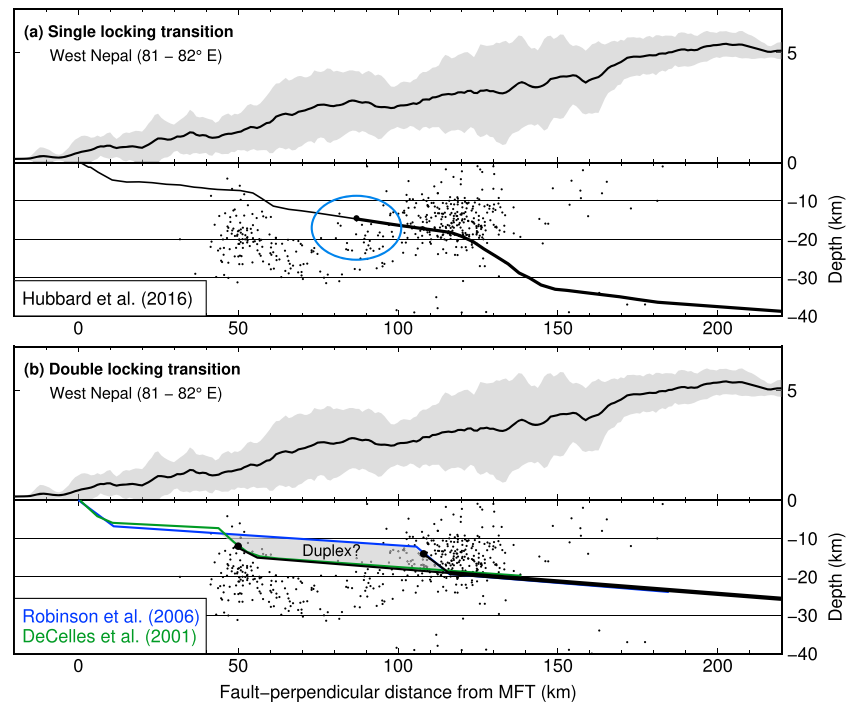


Figure 4. Illustration of two possibilities for interseismic strain accumulation in western Nepal (Figure 2a). (a) The structure proposed by Hubbard et al. (2016), similar to DeCelles et al. (1998), with two ramps linking three separate décollements. The geodetic data requires that the locking transition occurs somewhere along the central décollement in this case, shown as the transition between the thick black line (creeping) and thin line (locked/coupled). The model uncertainties in the location of the locking transition are shown as the blue ellipse. (b) The Main Himalayan Thrust MHT structures proposed by DeCelles et al. (2001) in green and Robinson et al. (2006) in blue. Harvey et al. (2015) suggested that both ramps could still be active, forming a duplex between them. The material in gray was formerly part of the downgoing plate but will now become part of the overriding plate, as slip transfers from the old ramp (right) to the newly formed ramp (left). In this case, interseismic strain could accumulate on both ramps simultaneously (medium-thickness black lines) if the thermally controlled locking transition is located at a depth intersected by both ramps. The geodetic data are presently unable to distinguish between these two possibilities, due the sparsity of GPS observations and a strong trade-off between the depth of interseismic deformation and the width of the transition zone. Both panels show microseismicity (black dots) from the relocated Nepal National Seismological Centre (NSC) catalog (1996–2008; Ader et al., 2012; Rajauri et al., 2013), along with mean, minimum, and maximum topography for the western profile, with a 6× vertical exaggeration. MFT = Main Frontal Thrust.

locked-to-creeping transition falls along a décollement, rather than on the ramp as observed elsewhere (Figure 4a). The locking transition in Nepal is believed to be thermally controlled (e.g., Ader et al., 2012), so it is generally more likely to occur where the fault dips more steeply through the geothermal gradient, but it is nevertheless possible that this transition could sometimes fall along a gently dipping portion of the fault instead. Because GPS observations in western Nepal are currently sparse, we are not able to constrain the width of the locking transition, which could help to resolve this question. In the near future, our best avenue for obtaining more detailed information about the distribution of interseismic strain in this region is likely InSAR observations of interseismic uplift (e.g., Grandin et al., 2012). At the same time, our results suggest a clearer set of criteria under which geologic observations might be used to predict the potentially seismogenic portion of continental thrust belts even where dense geodetic data are not available.

Our model does not assume that microseismicity is physically related to the interseismic coupling transition, but the generally close correlation between our inferred coupling location and the density of microseismicity does agree with the proposed physical connection (Ader et al., 2012; Pandey et al., 1995; Stevens & Avouac, 2015). In many of the profiles, most of the microseismicity is located just south of our inferred coupling transition (Figures 2, 3, and S4). Such a southward offset of the microseismicity would be expected if the brittle-ductile transition is located near the base of the midcrustal ramp, while the microseismicity occurs

primarily in the volume around the ramp (Ader et al., 2012). The density of microseismicity is a complex function of stressing rate, thermal structure, frictional properties, and deformation history and off-fault damage (e.g., Cattin & Avouac, 2000); our results in western Nepal highlight that it should not be taken in isolation as a strain rate marker.

3.2. Depth of Locking

The model depths referred to here are relative to an idealized horizontal surface, while geologic reconstructions are generally relative to sea level. Thus, our model depths may be slightly too shallow compared to these reconstructions. Models in which we allowed the depth to vary as a free parameter sometimes resulted in extremely shallow inferred depths, in many cases less than 10 km below the surface. Such a shallow depth is reflected in the relatively sudden transition between GPS velocities moving with the Indian plate and those converging toward it at nearly the full rate (Figure 2). However, a shallow locking depth is inconsistent with both the depth of the Gorkha earthquake (Avouac, 2015; Wang et al., 2017) and structural reconstructions of the MHT at depth (DeCelles et al., 2001; Hubbard et al., 2016; Robinson et al., 2006). These preferred shallow depths may be due to bias from the heterogeneous GPS data distribution, unmodeled variations in elastic modulus (e.g., Savage, 1998), strain from unmodeled shallow crustal faults, inelastic strain, viscoelastic effects (see below), or topographic effects (e.g., Thompson et al., 2015). This is an important question for future studies; however, there is only a weak correlation in our model results between the depths and the horizontal location of the coupling transition (Figure 2; supporting information Figure S5), so our results still provide a robust constraint on the horizontal location. To account for this uncertainty in locking depth, we vary the fixed locking depth in our models from 12 to 22 km and use the full range of depths to define the model uncertainties as shown in Figures 2 and 3.

3.3. Viscoelastic Effects

Viscoelastic models and postseismic and paleogeodetic observations show that geodetic velocities above a fault naturally vary over time throughout the earthquake cycle (e.g., Chuang & Johnson, 2011; Hetland & Hager, 2006; Meltzner et al., 2015; Tsang et al., 2015). While Nepal has generally been seismically quiescent during the period of geodetic observation modeled here (1990s–2015), large earthquakes in the past century may still be contributing a small postseismic signal that could affect the interseismic velocities. To test the possible magnitude of this effect, we modeled the viscoelastic deformation caused by the largest of these, the 1934 $M\sim 8.2$ –8.4 Nepal-Bihar earthquake (Chen & Molnar, 1977; Sapkota et al., 2013), using the finite difference code *Relax* 1.0.7 (Barbot, 2014; Barbot & Fialko, 2010a, 2010b). The result is shown in supporting information Figure S7. The maximum rate anomaly is 2.4 mm/year, directed northward for sites located just above the earthquake source area. Sites just to the north of the source area have similar rates, but directed southward. Thus, the potential late postseismic velocity anomaly is nearly symmetric about the downdip edge of the coseismic source, which approximately coincides with the interseismic locked-creeping transition. Because of this symmetry, any viscoelastic transient could have the effect of narrowing the strain profile but would not shift its center in either direction. Thus, while a residual viscoelastic transient from large megathrust earthquakes in Nepal could bias the inferred long-term slip rate (by making it appear too large) or the depth of the coupling transition (by making it appear too shallow), it should not bias the inferred horizontal location of the coupling transition. We note that the late postseismic velocity anomaly modeled here is different from the immediate postseismic deformation following the 2015 Gorkha earthquake, which is dominated by afterslip in the downdip area just to the north of the rupture zone and therefore has a much less symmetric pattern (e.g., Gualandi et al., 2017; Wang & Fialko, 2018; Zhao et al., 2017).

3.4. Slip Rate and Moment Deficit

One of the primary results of this study is an updated estimate of the long-term convergence rate on the MHT throughout Nepal (Figure 3). The average rate we obtain, 15.5 ± 2 mm/year, is lower than the most commonly cited rates (e.g., Lavé & Avouac, 2001; Stevens & Avouac, 2015). Below, we explore several possible reasons for this discrepancy and show that our result is less likely to be biased by modeling artifacts than previous studies. We infer that the long-term moment deficit rate on the MHT across Nepal is likely smaller than previously reported (e.g., Ader et al., 2012) and show that this helps to explain part of the apparent shortfall of paleoseismic moment release over the last $\sim 1,000$ years relative to geodetic moment (e.g., Bilham & Ambraseys, 2005; Stevens & Avouac, 2016).

The average convergence rate of 15.5 ± 2 mm/year for all 2D profiles across Nepal is within the range of published values from prior geodetic and geologic studies (e.g., see comparisons by Bettinelli et al., 2006; Feldl and Bilham, 2006; and Stevens and Avouac, 2015). In particular, it agrees well with the recent estimate of 15 mm/year by Zheng et al. (2017), who did not attempt to model the fault coupling but looked only at the absolute difference in convergence rate between India and southern Tibet. This rate is strongly constrained by the geodetic velocities in southern Tibet, which reach 15 mm/year relative to India only 200 km north of the frontal thrust (Figure 2). Beyond that distance, the contribution of elastic loading from the MHT is small, and any additional convergence must be accommodated on other structures, namely, conjugate strike-slip faults associated with eastward escape tectonics within Tibet (e.g., Taylor et al., 2003). It is therefore difficult to construct a model in which the MHT accumulates slip at a rate faster than the net convergence. Models with the deepest assumed locking depths show slightly higher convergence rates (16.4 ± 2 mm/year for a depth of 22 km) but do not fit the data as well (supporting information Figure S5).

A higher convergence rate could be possible if a several hundred kilometer-wide coupling transition zone is assumed (Feldl & Bilham, 2006), but this is unlikely given the absence of postseismic afterslip at large distances beneath central Tibet following the Gorkha earthquake (e.g., Mencin et al., 2016; Wang & Fialko, 2018; Zhao et al., 2017). Some studies may have overestimated the convergence rates by considering only data close to the zone of elastic strain accumulation (e.g., Grandin et al., 2012), resulting in a trade-off between the model slip rate and locking depth that is similar to a well-known effect in strike-slip fault settings (Lindsey & Fialko, 2013; Smith-Konter et al., 2011). We also note that because interseismic geodetic observations are not sensitive to the geometry of the locked portion of the fault, which will ultimately propagate coseismic slip to the surface, these convergence rates are an upper bound for the slip rate on the MFT proper; if shallow faults other than the MFT accommodate some of this convergence at the surface (e.g., Whipple et al., 2016; Wobus et al., 2005), the long-term slip rate of the MFT near the surface could be even lower.

Bettinelli et al. (2006) explored several types of models and found a range of best-fitting rates between 13.5 and 19 mm/year. They explained higher slip rates in their 3D model compared to 2D models by proposing a systematic bias caused by neglecting 3D effects in 2D models. We compared synthetic predictions for data along a 2D transect using our 2D dislocation model and a backslip model using a 3D fault matching the piecewise curvature along the Himalayan arc in the model of Bettinelli et al. (2006) but could not reproduce this proposed bias: the predicted horizontal velocities are nearly identical (supporting information Figure S8). We also constructed a 3D deep dislocation model matching the 3D geometry of Bettinelli et al. (2006) and fit a single convergence rate and direction to the data across Nepal and southern Tibet following their proposed method. We conducted this simple model for three available regional-scale compilations of GPS data from Stevens and Avouac (2015), Kreemer et al. (2014), and Zheng et al. (2017) and obtained average convergence rates of 14.7 ± 0.1 , 17.1 ± 0.1 , and 15.6 ± 0.1 mm/year for the three data sets, respectively, although in all cases the predicted azimuths of vectors fit the data poorly because this semi-3D model does not account for lateral spreading in Tibet (supporting information Figure S9). Three-dimensional effects could also impact the inferred slip rates to some degree if unmodeled fault-parallel motions contribute to an increased total slip rate on the megathrust with a slightly different rate. The unmodeled fault-parallel rates from our profiles (supporting information Figure S2) are generally less than 5 mm/year; nevertheless, they do exhibit a trend within some profiles, which could potentially bias the results.

A fully 3D model permits additional parameters to account for this transcurrent motion across the Himalayas (e.g., Murphy et al., 2014; Silver et al., 2015), as well as east-west extension within southern Tibet (Armijo et al., 1986). We therefore constructed a 3D backslip model using the Blocks software (Meade & Loveless, 2009), which estimates best-fitting fault slip rates and resulting rigid block motions simultaneously. We used several blocks in southern Tibet to account for the observed east-west extension and modeled the MHT with a locking depth of 15 km and a dip of 8° so that the locking line falls in approximately the same place as inferred from the 2D models. We found that the best-fitting convergence rates for the MHT across Nepal are 15.4 ± 1.2 mm/year, indistinguishable from our 2D results (Figure 5). We computed the best-fitting rates for three different data sets (Kreemer et al., 2014; Stevens & Avouac, 2015; Zheng et al., 2017) and found consistent results; the average convergence rate across Nepal is between 14.5 and 15.4 mm/year in all three cases (supporting information Figure S10).

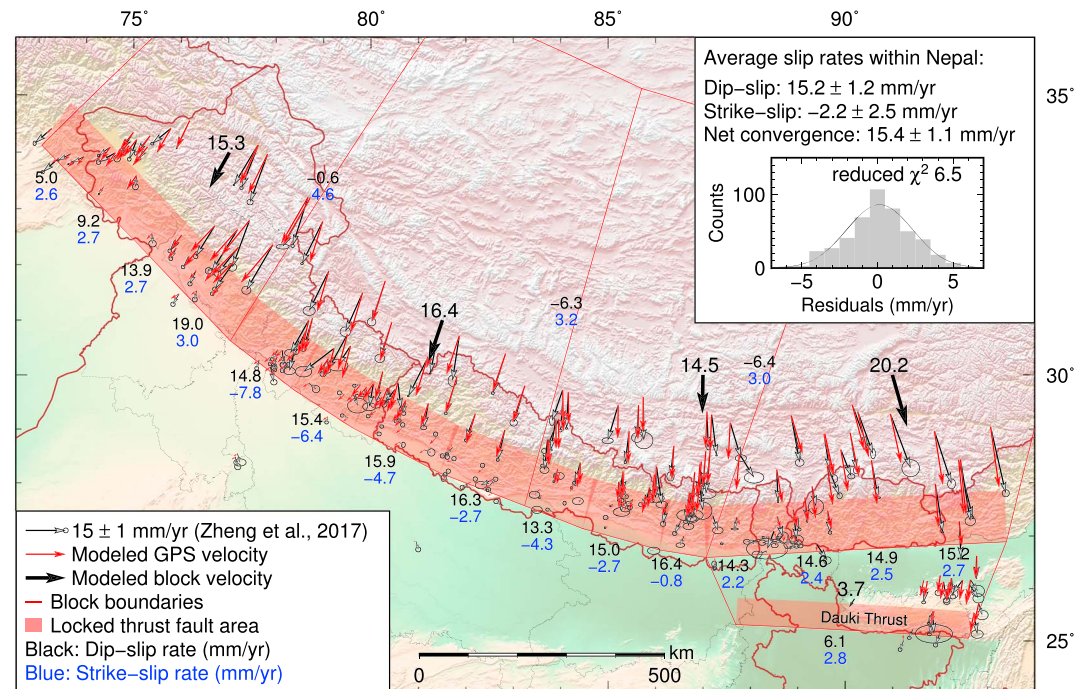


Figure 5. Block boundaries, modeled slip rates and block motions for a three-dimensional backslip model constructed using the blocks software (Meade & Loveless, 2009), using data from Zheng et al. (2017). Vectors show observed GPS velocities (black) and model prediction (red). Block motions, evaluated at one point inside each block, are shown as bold black arrows. Transparent red patches indicate the locked extent of the thrust faults. Dip-slip (convergence positive) rates are indicated in mm/year in black numbers; strike-slip rates (left-lateral positive) are shown in blue; formal uncertainties for all slip rates are 0.3 mm/year. Dip slip rates along the Main Frontal Thrust within Nepal range between 13.3 and 16.4 mm/year (weighted average 15.2 ± 1.2 mm/year), indistinguishable from the slip rates for the two-dimensional models. A faster convergence rate of the block in the far eastern Himalayas is divided between the Main Himalayan Thrust (MHT) and Dauki thrust, so that the MHT convergence rate remains relatively constant. West of 80°E, a larger strike-slip component and variable convergence rates may trade off with block rotation or other unmodeled overriding plate structures, owing to limited data coverage in this area.

Loveless and Meade (2011) considered block models for the Eurasian collision zone in which a geologic constraint was used to fix the MHT slip rate. We ran several models in which we applied a constraint of 20 ± 1 mm/year, taking the lower end of the range proposed by Lavé and Avouac (2001), but we found that the χ^2 misfit increased by 15–25% in this case (supporting information Figure S11). We conclude that it is possible that a different block geometry or other set of modeling choices could produce a higher best-fitting MHT slip rate, but such a model would need to invoke a mechanism to explain the low total convergence rates observed between southern Tibet and India (Zheng et al., 2017)—for example, the model of Loveless and Meade (2011) includes 4–8 mm/year of north-south-directed normal slip on the South Tibetan Detachment, which is inconsistent with geologic evidence that shows the cessation of north-south normal faulting in this area in the Miocene (Cannon & Murphy, 2014; Carosi et al., 2013).

Our best-fitting geodetic convergence rate in both 2D and 3D models is 10–30% smaller than the most commonly cited Holocene shortening rate estimated for Nepal based on geologic observations (Lavé & Avouac, 2001) but is consistent with other studies in the region (Bollinger et al., 2014; Mugnier et al., 2004). Lavé and Avouac (2001) used terrace uplift measurements to estimate a shortening rate of 21 ± 1.5 mm/year over the Holocene. Mugnier et al. (2004) used tilting measurements of dated Holocene surfaces, combined with balanced cross sections, to estimate a shortening rate of 14 ± 4 mm/year over the Holocene. Bollinger et al. (2014) calculated late Holocene uplift for several flights of terraces in eastern Nepal. While they do not quantitatively estimate an uplift or shortening rate, the best-fitting uplift rates to the data provided there are 7.8–8.1 mm/year, which represent approximate shortening rates of 15.6–16.2 mm/year given their assumed fault dip. The variation among these results could be caused purely by uncertainties in the

various methods used to estimate the rates, or it could point to the presence of medium-term variations in slip behavior on the megathrust over several earthquake cycles. For example, energy could be stored elastically near the deeper portion of the fault (e.g., Bilham et al., 2017), manifesting as temporarily reduced and subsequently accelerated rates of shallow slip in certain areas. At present, the temporal resolution of geologic observations and fidelity of numerical models is not yet sufficient to quantify the potential magnitude and timescales of this type of variability in megathrust behavior.

A lower MHT slip rate translates to a smaller inferred moment accumulation rate than previous studies (e.g., Ader et al., 2012; Stevens & Avouac, 2015). We compute the total moment accumulation rate for our 2D models by summing the nonoverlapping locked fault area multiplied by the slip rate for each profile along strike and find a total value of $4.8 \pm 0.3 \times 10^{19}$ Nm/year within Nepal, 27% less than the value found by Ader et al. (2012) over the same fault length of 1,000 km. This smaller value reduces, but does not eliminate, the proposed problem of a long-term seismic moment deficit inferred from paleoseismic observations (Ader et al., 2012; Bilham & Ambraseys, 2005; Bilham et al., 2017; Bollinger et al., 2014; Stevens & Avouac, 2016). This issue was partially addressed by Stevens and Avouac (2016), who assumed that their estimated moment deficit rate was overestimated by 50% due to a combination of unmodeled afterslip and interseismic modeling uncertainties; if we replace their estimated convergence rates with our lower inferred values, the data may be consistent either with a maximum earthquake magnitude smaller than 9.0, or a longer recurrence interval for such events. A lower MHT slip rate also affects the timing of inferred fault activation based on shortening estimates from balanced structural cross sections (e.g., Hubbard et al., 2016)—thus, these age estimates may need to be re-evaluated in this context.

4. Conclusions

We show that simple 2D models of interseismic deformation along the MHT in Nepal can illuminate detailed variations in the width of fault coupling along strike (Figure 2) and that they are not biased by potential 3D effects related to arc curvature and extension within Tibet (Figure 5). The results confirm that the deep transition from locked to creeping is likely controlled by the midcrustal ramp in eastern and central Nepal. By contrast, in western Nepal we find that the locking distance is intermediate between two proposed ramps, which could be related to the ongoing formation of a new sliver within a midcrustal duplex (Figure 4). The close correspondence between our geodetic results and the surface geology across Nepal suggests a promising avenue of research for other convergent zones where structural geologic observations may be more readily available than geodetic data.

One of the pressing earthquake hazard questions for the Himalayan convergence zone is the return time of large earthquakes along the MHT and their maximum potential magnitude. Our results, based on improved GPS observations and models, require an average convergence rate of 15.5 ± 2 mm/year and indicate that the suggested moment deficit of historical and paleoseismicity with respect to geodetic moment accumulation rates (Ader et al., 2012; Bilham & Ambraseys, 2005; Stevens & Avouac, 2016) is smaller than previously inferred—though we stress that the seismic hazard throughout the Himalayas remains high.

References

- Ader, T., Avouac, J. P., Liu-Zeng, J., Lyon-Caen, H., Bollinger, L., Galetzka, J., et al. (2012). Convergence rate across the Nepal Himalaya and interseismic coupling on the Main Himalayan Thrust: Implications for seismic hazard. *Journal of Geophysical Research*, *117*, B04403. <https://doi.org/10.1029/2011JB009071>
- Almeida, R., Lindsey, E. O., Bradley, K., Hubbard, J., Mallick, R., & Hill, E. M. (2018). Can the up-dip limit of frictional locking on megathrusts be detected geodetically? Quantifying the effect of stress shadows on near-trench coupling. *Geophysical Research Letters*, *45*. <https://doi.org/10.1029/2018GL077785>
- Armijo, R., Tapponnier, P., Mercier, J. L., & Tong-Lin, H. (1986). Quaternary extension in southern Tibet: Field observations and tectonic implications. *Journal of Geophysical Research*, *91*(B14), 13,803–13,872. <https://doi.org/10.1029/JB091iB14p13803>
- Avouac, J.-P. (2015). *Mountain building: From earthquakes to geologic deformation, Treatise on Geophysics* (Vol. 6). Amsterdam: Elsevier. <https://doi.org/10.1016/B978-0-444-53802-4.00120-2>
- Banerjee, P., Bürgmann, R., Nagarajan, B., & Apel, E. (2008). Intraplate deformation of the Indian subcontinent. *Geophysical Research Letters*, *35*, L18301. <https://doi.org/10.1029/2008GL035468>
- Barbot, S. (2014). RELAX v1.0.7 [software], computational infrastructure for geodynamics. Retrieved from <https://geodynamics.org/cig/software/relax/>
- Barbot, S., & Fialko, Y. (2010a). A unified continuum representation of post-seismic relaxation mechanisms: Semi-analytic models of afterslip, poroelastic rebound and viscoelastic flow: Semi-analytic models of postseismic transient. *Geophysical Journal International*, *182*(3), 1124–1140. <https://doi.org/10.1111/j.1365-246X.2010.04678.x>

Acknowledgments

This research was supported by the National Research Foundation Singapore under its Singapore NRF Fellowship scheme (NRF awards NRF-NRFF2010-064 and NRF-NRFF2013-06), by the Earth Observatory of Singapore (EOS), by the Singapore Ministry of Education (MOE) under the Research Centers of Excellence initiative, and by a Nanyang Technological University Startup grant. All GPS data used in the models presented here have been previously published and are listed in supporting information Table S1. This is EOS contribution number 190. We are grateful to V. Stevens for helpful reviews and to two reviewers of a previous version of this manuscript, to P. Tapponnier and J.-P. Avouac for helpful discussions, and to P. Adamek for linguistic advice, which significantly improved the structure of this paper. All data are available from references cited in the methods section; the GPS velocities used for our primary models are reproduced in supporting information Table S1.

- Barbot, S., & Fialko, Y. (2010b). Fourier-domain Green's function for an elastic semi-infinite solid under gravity, with applications to earthquake and volcano deformation: Fourier-domain elastic solutions. *Geophysical Journal International*, *182*(2), 568–582. <https://doi.org/10.1111/j.1365-246X.2010.04655.x>
- Bettinelli, P., Avouac, J.-P., Flouzat, M., Jouanne, F., Bollinger, L., Willis, P., & Chitrakar, G. R. (2006). Plate motion of India and interseismic strain in the Nepal Himalaya from GPS and DORIS measurements. *Journal of Geodesy*, *80*(8–11), 567–589. <https://doi.org/10.1007/s00190-006-0030-3>
- Bilham, R., & Ambraseys, N. (2005). Apparent Himalayan slip deficit from the summation of seismic moments for Himalayan earthquakes, 1500–2000. *Current Science*, *88*(10), 1658–1663. <http://www.jstor.org/stable/24110492>
- Bilham, R., Mencin, D., Bendick, R., & Bürgmann, R. (2017). Implications for elastic energy storage in the Himalaya from the Gorkha 2015 earthquake and other incomplete ruptures of the Main Himalayan Thrust. *Quaternary International*, *462*, 3–21. <https://doi.org/10.1016/j.quaint.2016.09.055>
- Bollinger, L., Sapkota, S. N., Tapponnier, P., Klinger, Y., Rizza, M., Van der Woerd, J., et al. (2014). Estimating the return times of great Himalayan earthquakes in eastern Nepal: Evidence from the Patu and Bardibas strands of the Main Frontal Thrust. *Journal of Geophysical Research: Solid Earth*, *119*, 7123–7163. <https://doi.org/10.1002/2014JB010970>
- Bradley, K. E., Feng, L., Hill, E. M., Natawidjaja, D. H., & Sieh, K. (2017). Implications of the diffuse deformation of the Indian Ocean lithosphere for slip partitioning of oblique plate convergence in Sumatra. *Journal of Geophysical Research: Solid Earth*, *122*, 572–591. <https://doi.org/10.1002/2016JB013549>
- Bürgmann, R., Kogan, M. G., Steblov, G. M., Hiley, G., Levin, V. E., & Apel, E. (2005). Interseismic coupling and asperity distribution along the Kamchatka subduction zone. *Journal of Geophysical Research*, *110*, B07405. <https://doi.org/10.1029/2005JB003648>
- Cannon, J. M., & Murphy, M. A. (2014). Active lower crustal deformation and Himalayan seismic hazard revealed by stream channels and regional geology. *Tectonophysics*, *633*(1), 34–42. <https://doi.org/10.1016/j.tecto.2014.06.031>
- Carosi, R., Montomoli, C., Rubatto, D., & Visonà, D. (2013). Leucogranite intruding the south Tibetan detachment in western Nepal: Implications for exhumation models in the Himalayas. *Terra Nova*. <https://doi.org/10.1111/ter.12062>
- Cattin, R., & Avouac, J. P. (2000). Modeling mountain building and the seismic cycle in the Himalaya of Nepal. *Journal of Geophysical Research*, *105*(B6), 13389–13407. <https://doi.org/10.1029/2000JB900032>
- Chen, W., & Molnar, P. (1977). Seismic moments of major earthquakes and the average rate of slip in central Asia. *Journal of Geophysical Research*, *82*(20), 2945–2969. <https://doi.org/10.1029/JB082i020p02945>
- Chlieh, M., Avouac, J. P., Sieh, K., Natawidjaja, D. H., & Galetzka, J. (2008). Heterogeneous coupling of the Sumatran megathrust constrained by geodetic and paleogeodetic measurements. *Journal of Geophysical Research*, *113*, B05305. <https://doi.org/10.1029/2007JB004981>
- Chuang, R. Y., & Johnson, K. (2011). Reconciling geologic and geodetic model fault slip-rate discrepancies in southern California: Consideration of nonsteady mantle flow and lower crustal fault creep. *Geology*, *39*(7), 627–630. <https://doi.org/10.1130/G32120.1>
- DeCelles, P. G., Gehrels, G. E., Quade, J., Ojha, T. P., Kapp, P. A., & Upreti, B. N. (1998). Neogene foreland basin deposits, erosional unroofing, and the kinematic history of the Himalayan fold-thrust belt, western Nepal. *Bulletin of the Geological Society of America*, *110*(1), 2–21. [https://doi.org/10.1130/0016-7606\(1998\)110%3C0002:NFBDEU%3E2.3.CO;2](https://doi.org/10.1130/0016-7606(1998)110%3C0002:NFBDEU%3E2.3.CO;2)
- DeCelles, P. G., Robinson, D. M., Quade, J., Ojha, T. P., Garzzone, C. N., Copeland, P., & Upreti, B. N. (2001). Stratigraphy, structure, and tectonic evolution of the Himalayan fold-thrust belt in western Nepal. *Tectonics*, *20*(4), 487–509. <https://doi.org/10.1029/2000TC001226>
- Department of Mines and Geology of Nepal (1994). Geologic map of Nepal 1:1,000,000.
- Elliott, J. R., Jolivet, R., Gonzalez, P. J., Avouac, J.-P., Hollingsworth, J., Searle, M. P., & Stevens, V. L. (2016). Himalayan megathrust geometry and relation to topography revealed by the Gorkha earthquake. *Nature Geoscience*, *9*(2), 174–180. <https://doi.org/10.1038/ngeo2623>
- Feldl, N., & Bilham, R. (2006). Great Himalayan earthquakes and the Tibetan plateau. *Nature*, *444*(7116), 165–170. <https://doi.org/10.1038/nature05199>
- Freytmüller, J., Bilham, R., Bürgmann, R., Larson, K. M., Paul, J., Jade, S., & Gaur, V. (1996). Global Positioning System measurements of Indian plate motion and convergence across the Lesser Himalaya. *Geophysical Research Letters*, *23*(22), 3107–3110. <https://doi.org/10.1029/96GL02518>
- Gahalaut, V. K., Kundu, B., Laishram, S. S., Catherine, J., Kumar, A., Singh, M. D., et al. (2013). Aseismic plate boundary in the Indo-Burmese wedge, northwest Sunda Arc. *Geology*, *41*(2), 235–238. <https://doi.org/10.1130/G33771.1>
- Galetzka, J., Melgar, D., Genrich, J. F., Geng, J., Owen, S., Lindsey, E. O., et al. (2015). Slip pulse and resonance of Kathmandu basin during the 2015 M_w 7.8 Gorkha earthquake, Nepal imaged with space geodesy. *Science*, *349*(6252), 1091–1095. <https://doi.org/10.1126/science.aac6383>
- Gao, R., Lu, Z., Klempner, S. L., Wang, H., Dong, S., Li, W., & Li, H. (2016). Crustal-scale duplexing beneath the Yarlung Zangbo suture in the western Himalaya. *Nature Geoscience*, *9*(7), 555–560. <https://doi.org/10.1038/ngeo2730>
- Grandin, R., Doin, M. P., Bollinger, L., Pinel-Puysségur, B., Ducret, G., Jolivet, R., & Sapkota, S. N. (2012). Long-term growth of the Himalaya inferred from interseismic InSAR measurement. *Geology*, *40*(12), 1059–1062. <https://doi.org/10.1130/G33154.1>
- Gualandi, A., Avouac, J.-P., Galetzka, J., Genrich, J. F., Blewitt, G., Adhikari, L. B., et al. (2017). Pre- and post-seismic deformation related to the 2015 M_w 7.8 Gorkha earthquake, Nepal. *Tectonophysics*, *714–715*, 90–106. <https://doi.org/10.1016/j.tecto.2016.06.014>
- Harvey, J. E., Burbank, D. W., & Bookhagen, B. (2015). Along-strike changes in Himalayan thrust geometry: Topographic and tectonic discontinuities in western Nepal. *Lithosphere*, *7*(5), 511–518. <https://doi.org/10.1130/L444.1>
- He, J., Vernant, P., Chery, J., Wang, W., Lu, S., Ku, W., et al. (2013). Nailing down the slip rate of the Altyn Tagh fault. *Geophysical Research Letters*, *40*, 5382–5386. <https://doi.org/10.1002/2013GL057497>
- Herman, F., Copeland, P., Avouac, J. P., Bollinger, L., Maheo, G., Le Fort, P., et al. (2010). Exhumation, crustal deformation, and thermal structure of the Nepal Himalaya derived from the inversion of thermochronological and thermobarometric data and modeling of the topography. *Journal of Geophysical Research*, *115*, B06407. <https://doi.org/10.1029/2008JB006126>
- Hetland, E., & Hager, B. (2006). Interseismic strain accumulation: Spin-up, cycle invariance, and irregular rupture sequences. *Geochemistry, Geophysics, Geosystems*, *7*, Q05004. <https://doi.org/10.1029/2005GC001087>
- Hubbard, J., Almeida, R., Foster, A., Sapkota, S. N., Bürgi, P., & Tapponnier, P. (2016). Structural segmentation controlled the 2015 M_w 7.8 Gorkha earthquake rupture in Nepal. *Geology*, *44*(8), 639–642. <https://doi.org/10.1130/G38077.1>
- Hyndman, R. D. (2013). Downdip landward limit of Cascadia great earthquake rupture. *Journal of Geophysical Research: Solid Earth*, *118*, 5530–5549. <https://doi.org/10.1002/jgrb.50390>
- Ischuk, A., Bendick, R., Rybin, A., Molnar, P., Khan, S. F., Kuzikov, S., et al. (2013). Kinematics of the Pamir and Hindu Kush regions from GPS geodesy. *Journal of Geophysical Research - Solid Earth*, *118*, 2408–2416. <https://doi.org/10.1002/jgrb.50185>

- Jackson, M., & Bilham, R. (1994). Constraints on Himalayan deformation inferred from vertical velocity fields in Nepal and Tibet. *Journal of Geophysical Research*, 99(B7), 13,897–13,912. <https://doi.org/10.1029/94JB00714>
- Jade, S., Bhatt, B. C., Yang, Z., Bendick, R., Gaur, V. K., Molnar, P., et al. (2004). GPS measurements from the Ladakh Himalaya, India: Preliminary tests of plate-like or continuous deformation in Tibet. *Geological Society of America Bulletin*, 116(11–12), 1385–1391. <https://doi.org/10.1130/B25357.1>
- Jade, S., Mukul, M., Bhattacharyya, A. K., Vijayan, M. S. M., Jaganathan, S., Kumar, A., et al. (2007). Estimates of interseismic deformation in Northeast India from GPS measurements. *Earth and Planetary Science Letters*, 263(3–4), 221–234. <https://doi.org/10.1016/j.epsl.2007.08.031>
- Jouanne, F., Mugnier, J. L., Gamond, J. F., Le Fort, P., Pandey, M. R., Bollinger, L., et al. (2004). Current shortening across the Himalayas of Nepal. *Geophysical Journal International*, 157(1), 1–14. <https://doi.org/10.1111/j.1365-246X.2004.02180.x>
- Kreemer, C., Klein, E., Shen, Z.-K., Wang, M., Estey, L., Wier, S., & Boler, F. (2014). A geodetic plate motion and Global Strain Rate Model. *Geochemistry, Geophysics, Geosystems*, 15, 3849–3889. <https://doi.org/10.1002/2014GC005407>
- Larson, K. M., Bürgmann, R., Bilham, R., & Freymueller, J. T. (1999). Kinematics of the India-Eurasia collision zone from GPS measurements. *Journal of Geophysical Research*, 104(B1), 1077–1093. <https://doi.org/10.1029/1998JB900043>
- Lavé, J., & Avouac, J. P. (2001). Fluvial incision and tectonic uplift across the Himalayas of central Nepal. *Journal of Geophysical Research*, 106(B11), 26,561–26,591. <https://doi.org/10.1029/2001JB000359>
- Liang, S., Gan, W., Shen, C., Xiao, G., Liu, J., Chen, W., et al. (2013). Three-dimensional velocity field of present-day crustal motion of the Tibetan Plateau derived from GPS measurements. *Journal of Geophysical Research: Solid Earth*, 118, 5722–5732. <https://doi.org/10.1002/2013JB010503>
- Lindsey, E. O., & Fialko, Y. (2013). Geodetic slip rates in the southern San Andreas fault system: Effects of elastic heterogeneity and fault geometry. *Journal of Geophysical Research: Solid Earth*, 118, 689–697. <https://doi.org/10.1029/2012JB009358>
- Lindsey, E. O., Natsuaki, R., Xu, X., Shimada, M., Hashimoto, M., Melgar, D., & Sandwell, D. T. (2015). Line-of-sight displacement from ALOS-2 interferometry: M_w 7.8 Gorkha earthquake and M_w 7.3 aftershock. *Geophysical Research Letters*, 42, 6655–6661. <https://doi.org/10.1002/2015GL065385>
- Lindsey, E. O., Sahakian, V. J., Fialko, Y., Bock, Y., Barbot, S., & Rockwell, T. K. (2014). Interseismic strain localization in the San Jacinto Fault Zone. *Pure and Applied Geophysics*, 171(11), 2937–2954. <https://doi.org/10.1007/s00024-013-0753-z>
- Loveless, J. P., & Meade, B. J. (2010). Geodetic imaging of plate motions, slip rates, and partitioning of deformation in Japan. *Journal of Geophysical Research*, 115, B02410. <https://doi.org/10.1029/2008JB006248>
- Loveless, J. P., & Meade, B. J. (2011). Partitioning of localized and diffuse deformation in the Tibetan Plateau from joint inversions of geologic and geodetic observations. *Earth and Planetary Science Letters*, 303(1–2), 11–24. <https://doi.org/10.1016/j.epsl.2010.12.014>
- Mahesh, P., Catherine, J. K., Gahalaut, V. K., Kundu, B., Ambikapathy, A., Bansal, A., et al. (2012). Rigid Indian plate: Constraints from GPS measurements. *Gondwana Research*, 22(3–4), 1068–1072. <https://doi.org/10.1016/j.gr.2012.01.011>
- Mahesh, P., Rai, S. S., Sivaram, K., Paul, A., Gupta, S., Sarma, R., & Gaur, V. K. (2013). One-dimensional reference velocity model and precise locations of earthquake hypocenters in the Kumaon-Garhwal Himalaya. *Bulletin of the Seismological Society of America*, 103(1), 328–339. <https://doi.org/10.1785/0120110328>
- Mansinha, L., & Smylie, D. E. (1971). The displacement fields of inclined faults. *Bulletin of the Seismological Society of America*, 61, 1433–1440.
- McCaffrey, R., & Nabelek, J. (1998). Role of oblique convergence in the active deformation of the Himalayas and southern Tibet plateau. *Geology*, 26(8), 691. [https://doi.org/10.1130/0091-7613\(1998\)026%3C0691:ROOCIT%3E2.3.CO;2](https://doi.org/10.1130/0091-7613(1998)026%3C0691:ROOCIT%3E2.3.CO;2)
- Melnick, D., Bookhagen, B., Strecker, M. R., & Echter, H. P. (2009). Segmentation of megathrust rupture zones from fore-arc deformation patterns over hundreds to millions of years, Arauco peninsula, Chile. *Journal of Geophysical Research*, 114, B01407. <https://doi.org/10.1029/2008JB005788>
- Meltzner, A. J., Sieh, K., Chiang, H.-W., Shen, C.-C., Suwargadi, B. W., Natawidjaja, D. H., et al. (2012). Persistent termini of 2004- and 2005-like ruptures of the Sunda megathrust. *Journal of Geophysical Research*, 117, B04405. <https://doi.org/10.1029/2011JB008888>
- Meltzner, A. J., Sieh, K., Chiang, H.-W., Wu, C.-C., Tsang, L. L. H., Shen, C.-C., et al. (2015). Time-varying interseismic strain rates and similar seismic ruptures on the Nias–Simeulue patch of the Sunda megathrust. *Quaternary Science Reviews*, 122, 258–281. <https://doi.org/10.1016/j.quascirev.2015.06.003>
- Moreno, M., Rosenau, M., & Oncken, O. (2010). 2010 Maule earthquake slip correlates with pre-seismic locking of Andean subduction zone. *Nature*, 467(7312), 198–202. <https://doi.org/10.1038/nature09349>
- Morgan, P. M., Feng, L., Meltzner, A. J., Lindsey, E. O., Tsang, L. L. H., & Hill, E. M. (2017). Sibling earthquakes generated within a persistent rupture barrier on the Sunda megathrust under Simeulue Island. *Geophysical Research Letters*, 44, 2159–2166. <https://doi.org/10.1002/2016GL071901>
- Mugnier, J., Huyghe, P., Leturmy, P., & Jouanne, F. (2004). Episodicity and rates of thrust-sheet motion in the Himalayas (western Nepal). In *Thrust Tectonics and Hydrocarbon System, AAPG Memoir*, (Vol. 82, pp. 91–114). Available at <http://archives.datapages.com/data/specpubs/memoir82/CHAPTER6/CHAPTER6.HTM>
- Mukul, M., Jade, S., Bhattacharyya, A., & Bhusan, K. (2010). Crustal shortening in convergent orogens: Insights from Global Positioning System (GPS) measurements in northeast India. *Journal of the Geological Society of India*, 75(1), 302–312. <https://doi.org/10.1007/s12594-010-0017-9>
- Mullick, M., Riguzzi, F., & Mukhopadhyay, D. (2009). Estimates of motion and strain rates across active faults in the frontal part of eastern Himalayas in North Bengal from GPS measurements. *Terra Nova*, 21(5), 410–415. <https://doi.org/10.1111/j.1365-3121.2009.00898.x>
- Murphy, M. A., Taylor, M. H., Gosse, J., Silver, C. R. P., Whipp, D. M., & Beaumont, C. (2014). Limit of strain partitioning in the Himalaya marked by large earthquakes in western Nepal. *Nature Geoscience*, 7(1), 38–42. <https://doi.org/10.1038/ngeo2017>
- Nakata, T., Yagi, H., Okumura, K., Upreti, B. N., Rockwell, T. K., Virid, N. S., et al. (1998). "First successful paleoseismic trench study on active faults in the Himalaya". Fall meeting, American Geophysical Union, San Francisco.
- Pandey, M. R., Tandukar, R. P., Avouac, J. P., Lavé, J., & Massot, J. P. (1995). Interseismic strain accumulation on the Himalayan crustal ramp (Nepal). *Geophysical Research Letters*, 22(7), 751–754. <https://doi.org/10.1029/94GL02971>
- Paul, J., Bürgmann, R., Gaur, V. K., Bilham, R., Larson, K. M., Ananda, M. B., et al. (2001). The motion and active deformation of India. *Geophysical Research Letters*, 28(4), 647–650. <https://doi.org/10.1029/2000GL011832>
- Ponraj, M., Miura, S., Reddy, C. D., Prajapati, S. K., Amirtharaj, S., & Mahajan, S. H. (2010). Estimation of strain distribution using GPS measurements in the Kumaun region of Lesser Himalaya. *Journal of Asian Earth Sciences*, 39(6), 658–667. <https://doi.org/10.1016/j.jseaes.2010.04.037>
- Qiu, Q., Hill, E. M., Barbot, S., Hubbard, J., Feng, W., Lindsey, E. O., et al. (2016). The mechanism of partial rupture of a locked megathrust: The role of fault morphology. *Geology*, 44(10), 875–878. <https://doi.org/10.1130/G38178.1>

- Rajaure, S., Sapkota, S. N., Adhikari, L. B., Koirala, B., Bhattarai, M., Tiwari, D. R., et al. (2013). Double difference relocation of local earthquakes in the Nepal Himalaya. *Journal of the Nepal Geological Society*, 46, 133–142.
- Rani, S., & Singh, S. J. (1992). Static deformation of a uniform half-space due to a long dip-slip fault. *Geophysical Journal International*, 109, 469–476.
- Robinson, D. M., DeCelles, P. G., & Copeland, P. (2006). Tectonic evolution of the Himalayan thrust belt in western Nepal: Implications for channel flow models. *Geological Society of America Bulletin*, 118(7–8), 865–885. <https://doi.org/10.1130/B25911.1>
- Segall, P. (2010). *Earthquake and volcano deformation*. Princeton University Press.
- Sapkota, S. N., Bollinger, L., Klinger, Y., Tapponnier, P., Gaudemer, Y., & Tiwari, D. (2013). Primary surface ruptures of the great Himalayan earthquakes in 1934 and 1255. *Nature Geoscience*, 6(1), 71–76. <https://doi.org/10.1038/ngeo1669>
- Savage, J. C. (1980). Dislocations in seismology. In F. R. N. Nabarro (Ed.), *Dislocations in solids* (pp. 251–339). New York: North-Holland Publishing.
- Savage, J. C. (1998). Displacement field for an edge dislocation in a layered half-space. *Journal of Geophysical Research*, 103(B2), 2439–2446. <https://doi.org/10.1029/97JB02562>
- Schelling, D., & Arita, K. (1991). Thrust tectonics, crustal shortening, and the structure of the far eastern Nepal Himalaya. *Tectonics*, 10(5), 851–862. <https://doi.org/10.1029/91TC01011>
- Scholz, C. H. (1988). The brittle-plastic transition and the depth of seismic faulting. *Geologische Rundschau*, 77(1), 319–328. <https://doi.org/10.1007/BF01848693>
- Scholz, C. H. (1998). Earthquakes and friction laws. *Nature*, 391(6662), 37–42. <https://doi.org/10.1038/34097>
- Silver, C. R. P., Murphy, M. A., Taylor, M. H., Gosse, J., & Baltz, T. (2015). Neotectonics of the Western Nepal Fault System: Implications for Himalayan strain partitioning. *Tectonics*, 34, 2494–2513. <https://doi.org/10.1002/2014TC003730>
- Smith-Konter, B. R., Sandwell, D. T., & Shearer, P. (2011). Locking depths estimated from geodesy and seismology along the San Andreas fault system: Implications for seismic moment release. *Journal of Geophysical Research*, 116, B06401. <https://doi.org/10.1029/2010JB008117>
- Stevens, V. L., & Avouac, J. P. (2015). Interseismic coupling on the Main Himalayan Thrust. *Geophysical Research Letters*, 42, 5828–5837. <https://doi.org/10.1002/2015GL064845>
- Stevens, V. L., & Avouac, J. P. (2016). Millenary $M_w > 9.0$ earthquakes required by geodetic strain in the Himalaya. *Geophysical Research Letters*, 43, 1118–1123. <https://doi.org/10.1002/2015GL067336>
- Suppe, J. (1983). Geometry and kinematics of fault-bend folding. *American Journal of Science*, 283(7), 684–721. <https://doi.org/10.2475/ajs.283.7.68>
- Suwa, Y., Miura, S., Hasegawa, A., Sato, T., & Tachibana, K. (2006). Interplate coupling beneath NE Japan inferred from three-dimensional displacement field. *Journal of Geophysical Research*, 111, B04402. <https://doi.org/10.1029/2004JB003203>
- Tang, G., Barton, P. J., McNeill, L. C., Henstock, T. J., Tilmann, F., Dean, S. M., et al. (2013). 3-D active source tomography around Simeulue Island offshore Sumatra: Thick crustal zone responsible for earthquake segment boundary. *Geophysical Research Letters*, 40, 48–53. <https://doi.org/10.1029/2012GL054148>
- Taylor, M., Yin, A., Ryerson, F. J., Kapp, P., & Ding, L. (2003). Conjugate strike-slip faulting along the Bangong-Nujiang suture zone accommodates coeval east-west extension and north-south shortening in the interior of the Tibetan Plateau. *Tectonics*, 22(4), 1044. <https://doi.org/10.1029/2002TC001361>
- Thompson, T. B., Plesch, A., Shaw, J. H., & Meade, B. J. (2015). Rapid slip-deficit rates at the eastern margin of the Tibetan Plateau prior to the 2008 M_w 7.9 Wenchuan earthquake. *Geophysical Research Letters*, 42, 1677–1684. <https://doi.org/10.1002/2014GL062833>
- Tsang, L. L. H., Meltzner, A. J., Hill, E. M., Freymueller, J. T., & Sieh, K. (2015). A paleogeodetic record of variable interseismic rates and megathrust coupling at Simeulue Island, Sumatra. *Geophysical Research Letters*, 42, 10,585–10,594. <https://doi.org/10.1002/2015GL066366>
- Wallace, L. M., Beavan, J., McCaffrey, R., & Darby, D. (2004). Subduction zone coupling and tectonic block rotations in the North Island, New Zealand. *Journal of Geophysical Research*, 109, B12406. <https://doi.org/10.1029/2004JB003241>
- Wang, K., & Fialko, Y. (2018). Observations and modeling of coseismic and postseismic deformation due to the 2015 M_w 7.8 Gorkha (Nepal) earthquake. *Journal of Geophysical Research: Solid Earth*, 123, 761–779. <https://doi.org/10.1002/2017JB014620>
- Wang, X., Wei, S., & Wu, W. (2017). Double-ramp on the Main Himalayan Thrust revealed by broadband waveform modeling of the 2015 Gorkha earthquake sequence. *Earth and Planetary Science Letters*, 473, 83–93. <https://doi.org/10.1016/j.epsl.2017.05.032>
- Wesnousky, S. G., Kumahara, Y., Chamlagain, D., Pierce, I. K., Reedy, T., Angster, S. J., & Giri, B. (2017). Large paleoearthquake timing and displacement near Damak in eastern Nepal on the Himalayan Frontal Thrust. *Geophysical Research Letters*, 44, 8219–8226. <https://doi.org/10.1002/2017GL074270>
- Whipple, K. X., Shirzaei, M., Hodges, K. V., & Ramon Arrowsmith, J. (2016). Active shortening within the Himalayan orogenic wedge implied by the 2015 Gorkha earthquake. *Nature Geoscience*, 9(9), 711–716. <https://doi.org/10.1038/ngeo2797>
- Wobus, C., Heimsath, A., Whipple, K., & Hodges, K. (2005). Active out-of-sequence thrust faulting in the central Nepalese Himalaya. *Nature*, 434(7036), 1008–1011. <https://doi.org/10.1038/nature03499>
- Zhang, P. Z., Shen, Z., Wang, M., Gan, W., Bürgmann, R., Molnar, P., et al. (2004). Continuous deformation of the Tibetan Plateau from global positioning system data. *Geology*, 32(9), 809–812. <https://doi.org/10.1130/G20554.1>
- Zhao, B., Bürgmann, R., Wang, D., Tan, K., Du, R., & Zhang, R. (2017). Dominant controls of down-dip afterslip and viscous relaxation on the postseismic displacements following the M_w 7.9 Gorkha, Nepal earthquake. *Journal of Geophysical Research*, 122, 8376–8401. <https://doi.org/10.1002/2017JB014366>
- Zheng, G., Wang, H., Wright, T. J., Lou, Y., Zhang, R., Zhang, W., et al. (2017). Crustal deformation in the India-Eurasia collision zone from 25 years of GPS measurements. *Journal of Geophysical Research: Solid Earth*, 122, 9290–9312. <https://doi.org/10.1002/2017JB014465>